

Application of Graphene and Pyridine in Anode Modification for Enhanced Performance of Microbial Fuel Cells

Kun Cao

Department of Chemistry & Chemical Engineering, Neijiang Normal University, Neijiang, Sichuan, 641112, PR China

E-mail: kevin_cao0811@126.com

Received: 28 June 2016 / Accepted: 23 March 2017 / Published: 12 May 2017

Carbon cloth was modified by graphene oxide, and then electropolymerized 2,6-Pyridinedicarboxylic acid (PDC) on the treated carbon cloth, which was as anode for microbial fuel cells. The power density of the modified carbon cloth reaches $1035 \text{ mW}\cdot\text{m}^{-2}$, which was 3.2 times larger than that of the MFCs with the unmodified carbon cloth anode. BET, scanning electron microscopy (SEM) and Raman spectroscopy were employed to detect the surface characteristics of the carbon cloth. CV and electrochemical impedance spectroscopy (EIS) were used to confirm the electrochemical characteristics. The results showed that graphene oxide and PDC could improve the charge transfer performance and bacterial reproduction.

Keywords: Microbial fuel cells, electropolymerized, Electrochemically reducing graphene oxide, Pyridinedicarboxylic

1. INTRODUCTION

Microbial fuel cells (MFCs) are novel electrochemical devices that oxidize organic matter and generate electricity by combining microbial technology and electrochemical technology. Because of integrating features of two kinds of technologies, MFCs have been considered as a promising material and applied in extensive fields, such as wastewater treatment [1-4], implantable medical devices [5], energy recovery [6] and biosensors [7-9]. Nevertheless, the low power density of MFCs restricts the method to be adopted in more extensive fields.[10,11]. The factors affecting the MFCs performance in a low power density include cell design, inoculum, substrate, proton exchange material and electrode materials, etc. [12-18]. Materials of anode play a dominating role in the power generation and electron

transfer by determining the actual access area for microbe to anchor. Hence, a high-performance anode material is critical to improve the power output of MFCs.

The characteristics of the anode surface, such as surface area, surface potential, surface biocompatibility and surface roughness, significantly affect the anodic reaction's performance. As a matter of fact, many laboratory studies reported that nanostructured materials have been proven to be a very suitable matrix for modifying the electrode. It has been proved that after the use of carbon nanotube [19,20], polyaniline [21] and polypyrrole [22], the energy loss of modified MFCs electrodes decreased and the output of modified MFCs increased significantly. Pyridine's use as biosensors [23] was much focused and studied because of its excellent stability and biocompatibility, while reports or studies on MFCs electrode with pyridine had hardly aroused enough attention. This is one of reasons that motivate the author to create.

Graphene is the basic unit of all graphitic carbons with a single-atom-thick sheet consisting of sp^2 hybridized carbon atoms. As graphene has unique nanostructure, high surface area [27], and outstanding advantages in conductivity [28], mechanical strength [29] and electrocatalytic activities, it has showed great potentials in applications in extensive fields, such as lithium ion batteries [24], solar cells [25] and electrochemical super-capacitors [26]. Two methods can be taken to modify the electrodes by graphene. The first is directly deposition, which is to drop chemical reduction of graphene oxide (CRGNO) solution onto a conductive substrate [30,31]. The second way to reduce the GNO is electrochemical method (ERGNO), in this case, the thickness of the ERGNO films can be controllable as well as nontoxic.

In the present work, ERGNO/CC anode was fabricated by cyclic voltammetry (CV) method, the scanning potential from 0 to -1.6 V vs. a saturated calomel electrode (SCE) in phosphate buffer solution (PBS), and then, 2,6-Pyridinedicarboxylic acid (PDC) was electropolymerized on the surface of ERGNO/CC, and later adopted as MFCs anode. In order to verify the performance of PDC-ERGNO/CC and ERGNO/CC anodes, the properties of the modified anodes were examined by EIS and CV. Meanwhile, the surface characteristic was detected by Raman spectroscopy and SEM. In addition, the power output and the maximum power density were obtained as well.

2. EXPERIMENTAL

2.1. Chemicals and materials

Graphite oxide (GO) was purchased from a Nanjing technology company, and prepared according to Hummers' method [32]. CC and Nafion 117 (Dupont, USA) membrane were supplied by Shanghai Hesen Electric Co. Ltd. All chemicals were set at AR grade and used though not purged further. All of the solutions had been prepared with deionized water. Graphene oxide (GNO) was dispersed in water by the ultrasound equipment for 3 h and the concentration is $1 \text{ mg}\cdot\text{mL}^{-1}$. The upper brown dispersion was settled 7 days to avoid any unexfoliated graphite oxide. Besides, PDC was supplied by Aladdin Industrial Corporation.

2.2. Electrode fabrication

Prior to use, CC was cut into squares of 2 cm× 2 cm and then degreased in acetone for 3 h, later rinsed with the deionized water, and then, immersed in the sulfuric acid and nitric acid mixed solution ($V_{\text{sulfuric}} : V_{\text{nitric}} = 3 : 1$) for 3 h, then rinsed with deionized water a second time until the pH closes to neutral, finally, it took 12 h to dry the wet CC in a vacuum drying oven. The GNO/CC was prepared by dripping 1 mg·mL⁻¹ GNO dispersion on the CC surface layer by layer, then, dried by airing. Finishing all above, the weight gain of the GNO reached 2 mg [20]. Through CV method, GNO/CC was reduced. In such way, the ERGNO/CC was also prepared. PDC-ERGNO/CC was prepared by pulse electropolymerization in the PDC solution (0.01 mol·L⁻¹ PDC, 0.5 mol·L⁻¹ KCl), pulse voltage was set at 1.8V, pulse time was set at 0.7 s ($t_{\text{on}}=0.4$ s, $t_{\text{off}}=0.3$ s), then rinsed with the deionized water and dried.

2.3. MFCs construction and operation

Two polymethylmethacrylate cylinders (5 cm deep, 30 cm² of the cross sectional area) were used as MFCs reactor. The two chambers were separated by Nafion 117 membrane, each cell chamber has an effective volume of 150 mL. Original *Escherichia coli*(JM 109, Hongkong University) was grown at 37 °C for 24 h. Before inoculation, anode chamber with anolyte was saturated with nitrogen for 20 min and sterilisation. After that, 5 mL of *Escherichia coli* culture was inoculated. Anolyte consisted of 1 g·L⁻¹ C₆H₁₂O₆, 0.3 g·L⁻¹ NH₄Cl, 1g·L⁻¹ NaCl, 0.04 g·L⁻¹ CaCl₂·2H₂O, 0.3 g·L⁻¹ MgSO₄, 0.2 g·L⁻¹ NaHCO₃, 10.7 g·L⁻¹ K₂HPO₄, 5.3 g·L⁻¹ KH₂PO₄, and 1 mL trace elements [20]. CC (2 cm× 2 cm) without treatment was used as the cathode. 50 mmol/L K₃[Fe(CN)₆] and 100 mmol/L PBS were added in the cathodic chambers. The cell systems were placed in an incubator at 37±0.5°C and the anolyte was renewed by batch feeding when the potential lower than 50 mV.

2.4. Measurement and analysis

The CV was performed using the PARSTAT 2273 Potentiostat/Galvanostat (Princeton Applied Research) with 5 mV·s⁻¹ in a three-electrode cell system. The modified CC, SCE and the platinum plate were functioned as the working electrode, the reference and counter electrode, respectively. The impedance measurements were carried on at the frequency from 100 kHz to 10 mHz with a peak-to-peak under the open circuit potential (OCP) conditions with a 10 mv peak-to-peak sine wave as the excitation signal. The cell voltage was measured at a time interval of 10 min by a multichannel data recorder with a 1000 Ω external resistance connected unless otherwise specified. After changing the output load resistor over a range from 100 to 9999 Ω when the MFCs current stably, the power output curves' measurement were also carried on as well. Raman spectra measurement was carried out on a LabRAM HR Evolution. The specific surface area of CC, ERGNO/CC and PDC-ERGNO/CC were calculated by BET method (American Quautachrome Autosorb IQ2) and the microstructure of the electrodes were characterized by SEM (Hitachi S-3400N).

3. RESULTS AND DISCUSSION

3.1. Modification process of anode

Fig. 1 shows the CV curves of the electrochemical reduction of GNO/CC. The cathodic reduction peak from -0.58 to -1.5 V owing to the formation of ERGNO on the CC surface. The result is in accordance with the previous literature [33,34,35].

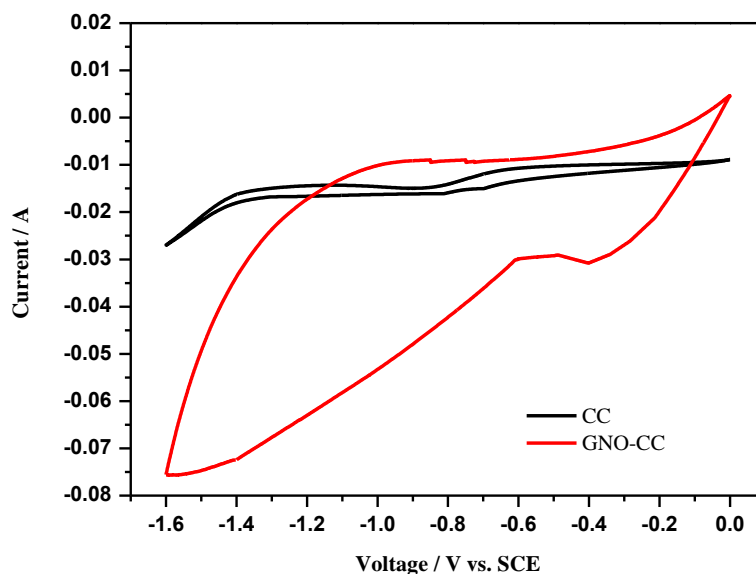


Figure 1. CV curves of CC and GNO/CC in PBS

Fig. 2 shows the current-time curves during pulse electropolymerization of PDC film from $0.01 \text{ mol}\cdot\text{L}^{-1}$ PDC monomer and $0.5 \text{ mol}\cdot\text{L}^{-1}$ KCl mixed solution. The first pulse from this figure, the current increases to 0.102 A within 0.4 s . In the pulse-on time ($t_{\text{on}}=0.4 \text{ s}$), the PDC monomer around the working electrode is oxidized into active monomer and some of active monomers electropolymerized into large molecules, which attached to the surface of ERGNO/CC through chemical bonds. The current becomes smaller, due to the decreasing concentration of monomer around the surface. In pulse-off time ($t_{\text{off}}=0.3 \text{ s}$), the active PDC monomers are polymerized and soak into the working electrode [36,37].

In order to know the mechanism of the polymerization, electrochemical quartz crystal microbalance was used to detect the process of polymerization. Fig. 3(A) is the voltage-time and quality-time curves of pulse electropolymerization at the first 10 s . Fig. 3(B) is the total mass-time curve of pulse electropolymerization. From Fig. 3(A), the instantaneous loading of film is $2.51 \mu\text{g}\cdot\text{cm}^{-2}$ at the pulse-on time, while is $30.09 \mu\text{g}\cdot\text{cm}^{-2}$ at pulse-off time. The quality increase of the PDC film should be slowly and regularly, which is consistent with the average loading of $2.51 \mu\text{g}\cdot\text{cm}^{-2}$ at pulse-on time. There are few active monomer polymerized into large molecules and chemically attached to the surface of ERGNO/CC. At the pulse-off time, active monomer around the working electrode polymerized into macromolecules and soaked into electrode temporarily, resulting in the increase of

$30.09 \mu\text{g}\cdot\text{cm}^{-2}$ instantly. Fig. 3(B) shows that, the quality increases with increasing polymerization time. The quality increases slowly at the beginning, due to the rate of macromolecules connecting to the surface lower than the polymerization rate. The activities connecting to the surface increase with increasing polymerization time, so the number of macromolecules connecting to the surface increases. After polymerization, the increased quality of the film is $16.96 \mu\text{g}\cdot\text{cm}^{-2}$.

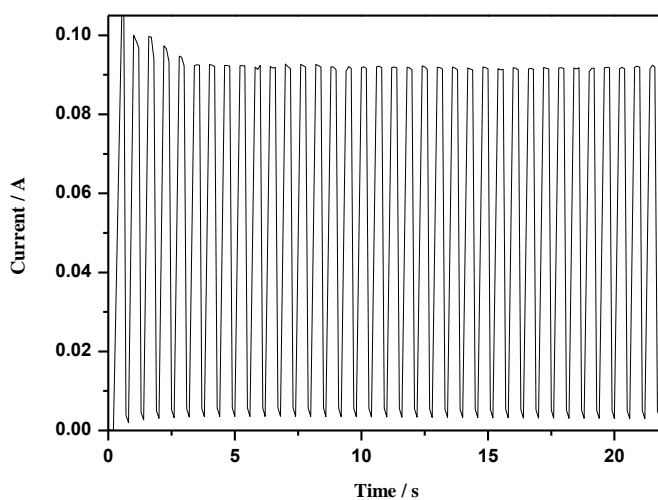


Figure 2. Current-time curves during unipolar pulse electropolymerization of PDC films

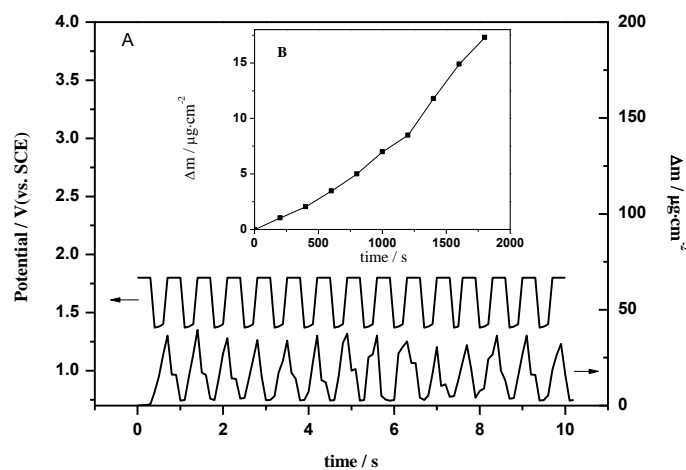


Figure 3. A: Potential-time and mass-time curves during pulse electropolymerization of PDC films. B: apparent mass of PDC films vs. time during pulse electropolymerization of PDC films.

3.2. Morphology analysis

In order to confirm whether the specific surface area has been modified by both ERGNO and PDC, we conduct the N_2 adsorption/desorption's measurements. Table 1 lists and shows the changes of the BET surface areas of different electrodes vividly. The surface area of CC is $2.87 \text{ m}^2/\text{g}$ and increase to $647 \text{ m}^2/\text{g}$ with ERGNO modified or $863 \text{ m}^2/\text{g}$ modified by PDC-ERGNO.

Table 1. BET surface area of different electrodes

Electrode	BET surface area (m ² /g)
CC	2.87
ERGNO/CC	647
PDC-ERGNO/CC	863

Fig. 4 is the SEM morphology of PDC-ERGNO/CC, ERGNO/CC and unmodified CC to examine the differences of anode surfaces after different treatments. From Fig. 4(a), the unmodified CC shows relatively smooth surface. Compared with Fig. 4(a), Fig. 4(b) (c) appears a large amount of micro structures, such as thin wrinkled and crumpled structures, that are typical structures of ERGNO, proving and responding to those results agreeably [34,38,39]. Fig. 4(c) also shows the film and particles between the carbon fiber. Obviously, it further proves that the PDC-ERGNO hybrid coating was formed on CC.

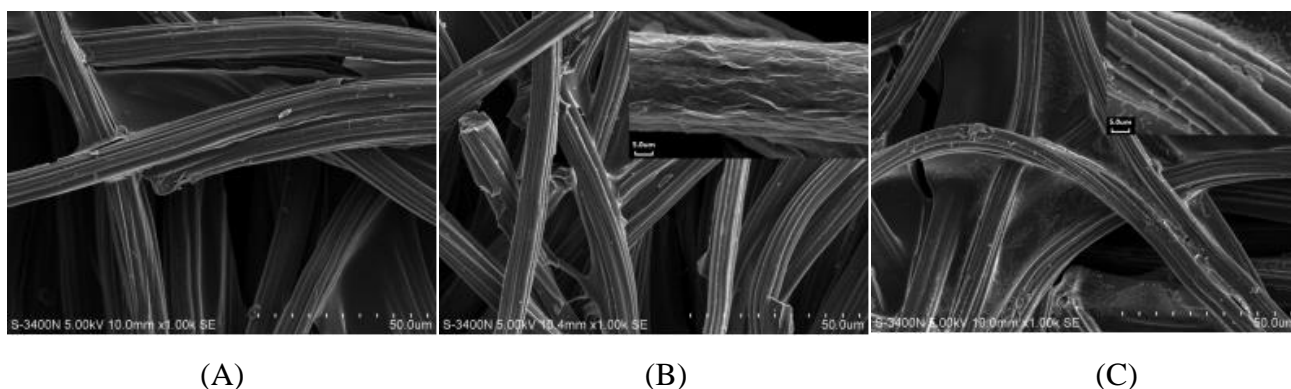
**Figure 4.** SEM images of CC (a), ERGNO/CC (b), and PDC-ERGNO/CC (c)

Fig. 5 shows the Raman spectra of the unmodified CC, ERGNO/CC and PDC-ERGNO/CC. The Raman spectrum of carbon cloth shows two peaks at 1346 cm⁻¹ and 1589 cm⁻¹ corresponding to the disordered (D) and graphitic (G) bands of CC, respectively [40]. The D peak and G peak of the ERGNO/CC and PDC-ERGNO/CC are appeared at 1348 cm⁻¹ at 1592 cm⁻¹. The intensity ratio of D/G increases after the GNO reduced electrochemically. This may be due to the number of sp³ bonding carbon atoms increased significantly, and the order degree was decreased [41,42]. For pure PDC, Raman peaks appeared at 997, 1152, 1293 and 1573 cm⁻¹, assign to pyridine ring breathing vibration peak, C-O stretching peak, O-H in-plane vibration peak and C bond-stretching peak, respectively [43]. In the case of PDC-ERGNO/CC, the appearance of these new peaks at 1001, 1179 cm⁻¹, which is the pattern of the PDC.

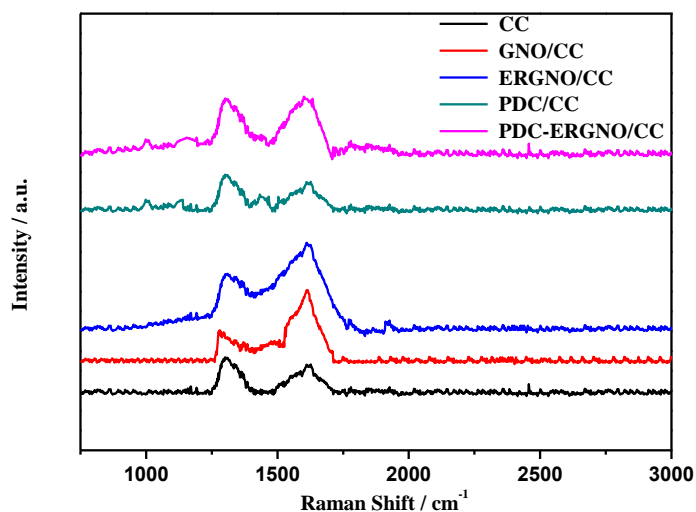


Figure 5. Raman spectrum of CC, GNO/CC, ERGNO/CC, PDC/CC and PDC-ERGNO/CC

3.3. Electrochemical analysis

Fig. 6 shows the CV test to indicate the electrochemical properties of the anode materials. From Fig. 6, the increase in the currents reflex that more surface area is involved for *E. Coli* attachment [30,31].

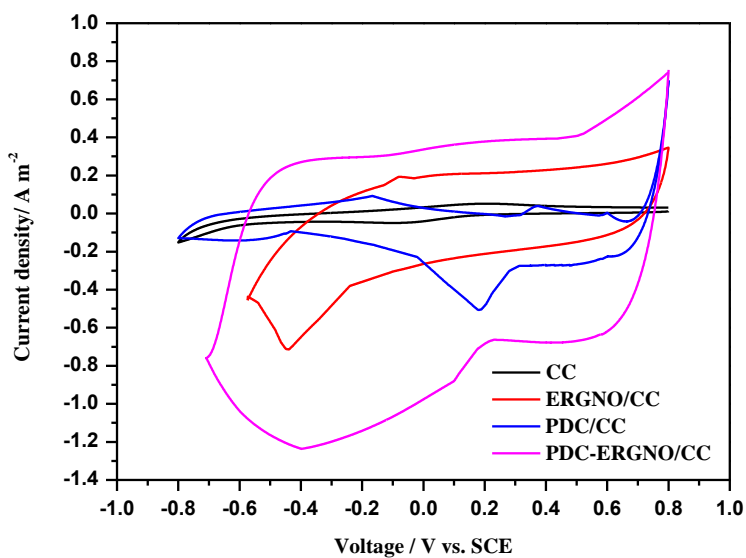


Figure 6. CVs of PDC-ERGNO/CC, ERGNO/CC, PDC/CC and CC in 100 mM PBS

Nyquist plots were employed to understand charge transferring process (Fig. 7). The impedance spectra exhibit similar characteristics as two clear parts: the depressed capacitive loop at the high frequencies and the straight line standing for changes under the environment of low

frequencies, which indicate the charge transfer and Warburg diffusion limitations, respectively. Considering the charge-transfer kinetic at the higher frequency as well as the diffusion at the lower frequency, the impedance data could be appropriately interpreted using the Randles equivalent circuit, in which R_s represents the solution resistance between the working electrode and the reference electrode, R_{ct} is the charge-transfer resistance, C_{dl} is the double layer capacitance, W is the Warburg impedance. In comparison with the CC anode, the semicircles of the modified anodes are notably smaller[44]. The R_{ct} of the PDC-ERGNO/CC and ERGNO/CC anodes are 37 Ω and 56 Ω , while it is 152 Ω for the CC anode, due to the reduction of internal resistance for the CC anode by PDC and ERGNO. Thus, the electrochemical performance of CC anode has been improved to a great extent due to treat the anode surface with the PDC-ERGNO.

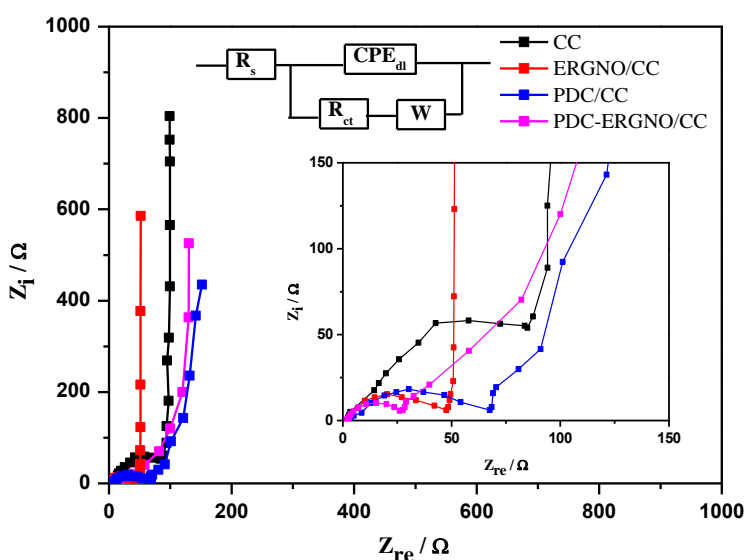


Figure 7. EIS of PDC-ERGNO/CC, ERGNO/CC, PDC/CC and CC in 100 mM PBS

3.4. Power curve

The power density output of the MFCs could be greatly improved as a result of enlarging area of specific surface and promoting efficiency of charge transferring by modified with PDC and ERGNO. To verify this, the performance of the MFCs was operated simultaneously with an external resistance of 1000 Ω . Fig. 8 also indicates that the power density of the PDC-ERGNO/CC and ERGNO/CC MFCs increases rapidly and stabilize at 870 $\text{mW}\cdot\text{m}^{-2}$ and 633.5 $\text{mW}\cdot\text{m}^{-2}$ and decreases due to depletion of organic matter in anolyte. As shown in Fig. 9, the open circuit potential (OCP) of the PDC-ERGNO/CC anode MFCs is 0.77 V, larger than that of the ERGNO/CC and the CC anode MFCs. Actually the OCP is dependent on electrochemical processes as well as biological in MFCs system [45]. In addition, all parameters are controlled except the anode. Power density of PDC-ERGNO/CC MFCs reaches max 1035 $\text{mW}\cdot\text{m}^{-2}$ at the current density of 1.92 $\text{A}\cdot\text{m}^{-2}$. In contrast, such power density of ERGNO/CC MFCs is 782 $\text{mW}\cdot\text{m}^{-2}$ with the current density of 2.25 $\text{A}\cdot\text{m}^{-2}$. The PDC-ERGNO/CC and ERGNO/CC anodes can apparently improve the MFCs power output 3.2 and 2.4

times whereas the maximum power density of unmodified MFCs fixing at only $327 \text{ mW}\cdot\text{m}^{-2}$ under similar situation.

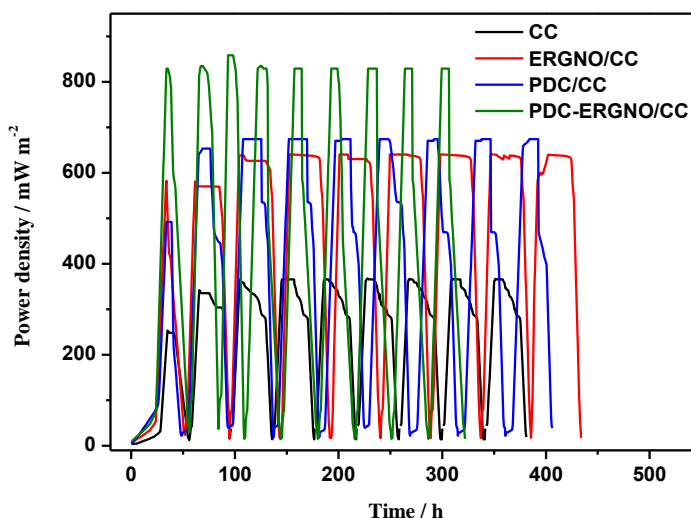


Figure 8. Power density output of the MFCs with PDC-ERGNO/CC, ERGNO/CC, PDC/CC and CC

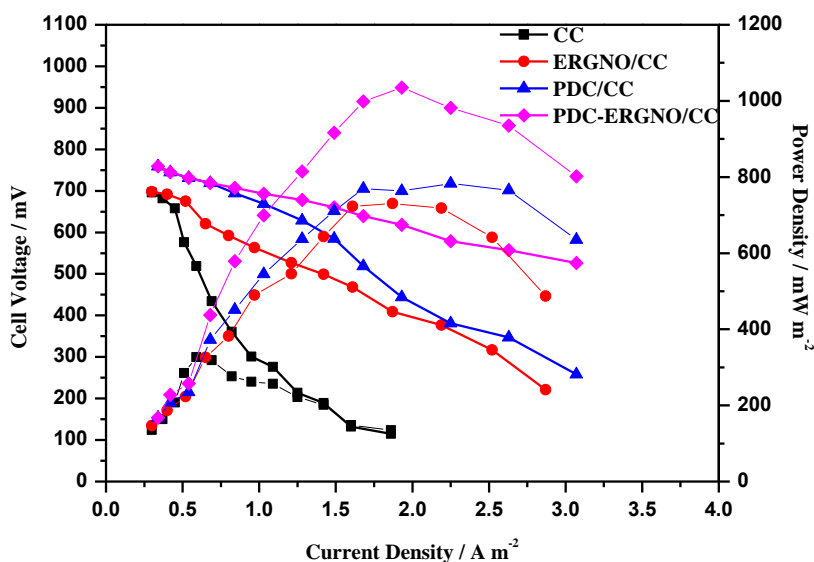


Figure 9. Polarization curves with PDC-ERGNO/CC, ERGNO/CC, PDC/CC and CC as the MFCs anodes

4. CONCLUSIONS

Reduction of graphene oxide in electrochemical ways is controllable and reproducible, the thickness is uniform, and moreover, toxic chemicals can be excluded. The maximum power density of the MFCs with PDC-ERGNO/CC anode achieved $1035 \text{ mW}\cdot\text{m}^{-2}$ which is 3.2 times larger than that the MFCs with the CC anode. The PDC-ERGNO modified anode could improve circumstances of the

surface area of the electrode, adhesiveness of microbe and efficiency of charge transferring. These results prove that the method provided within this paper is simple and reliable for fabricating new low-cost, nontoxic and effective anodes for MFCs.

ACKNOWLEDGEMENTS

The author gratefully acknowledges the support of Doctor Founding of Neijiang Normal University (No. 15B13).

References

1. C. Abourached, M. J. English and H. Liu, *J. Clean. Prod.*, 137 (2016) 144.
2. I. M. Jimenez, V. Celorrio, D. J. Fermin, J. Greenman and I. Ieropoulos, *Water Res.*, 109 (2017) 46.
3. Y. H. Li, L. F. Liu and F. L. Yang, *J. Membrane Sci.*, 525 (2017) 202.
4. G. Hernández-Flores, H. M. Poggi-Varaldo, O. Solorza-Feria, *Int. J. Hydrogen Energy*, 41 (2016) 23354.
5. S. H. Chang, J. S. Liou, J. L. Liu, Y. F. Chiu, C. H. Xu, B. Y. Chen and J. Z. Chen, *J. Power Sources*, 336 (2016) 99.
6. B. E. Logan and K. Rabaey, *Science*, 337 (2012) 686.
7. I. S. Chang, J. K. Jang, G. C. Gil, M. Kim, H. J. Kim, B. W. Cho and B. H. Kim, *Biosens. Bioelectron.*, 19 (2004) 607.
8. J. L. Zheng, C. X. Cheng, J. Zhang and X. H. Wu, *Int. J. Hydrogen Energy*, 41 (2016) 23156.
9. S. Luo and Z. He, *Electrochim. Acta*, 222 (2016) 338.
10. Z. Baicha, M. J. Salar-Garcia, V. M. Ortiz-Martinez, F. J. Hernandez-Fernandez, A. P. de los Rios, N. Labjar, E. Lotfi and M. Elmahi, *Fuel Process. Technol.*, 154 (2016) 104.
11. C. Y. Zhang, P. Liang, X. F. Yang, Y. Jiang, Y. H. Bian, C. M. Chen, X. Y. Zhang and X. Huang, *Biosens. Bioelectron.*, 81 (2016) 32.
12. S. Srikanth, M. Kumar, D. Singh, M. P. Singh and B. P. Das, *Bioresource Technol.*, 221 (2016) 70.
13. Y. J. Li, L. F. Liu, J. D. Liu, F. L. Yang and N. Q. Ren, *Desalination*, 349 (2014) 94.
14. V. M. Ortiz-Martinez, I. Gajda, M. J. Salar-Garcia, J. Greenman, F. J. Hernandez-Fernandez and I. Ieropoulos, *Chem. Eng. J.*, 291 (2016) 317.
15. J. Y. An, Y. S. Lee, T. Y. Kim and I. S. Chang, *J. Power Sources*, 323 (2016) 23.
16. D. J. Lee, J. S. Chang and J. Y. Lai, *Bioresource Technol.*, 198 (2015) 891.
17. C. S. He, Z. X. Mu, H. Y. Yang, Y. Z. Wang, Y. Mu and H. Q. Yu, *Chemosphere*, 140 (2015) 12.
18. Z. Fu, L. T. Yan, K. X. Li, B. C. Ge, L. T. Pu and X. Zhang, *Biosens. Bioelectron.*, 74 (2015) 989.
19. X. Xie, G. H. Yu, N. Liu, Z. A. Bao, C. S. Criddle and Y. Cui, *Energy Environ. Sci.*, 5 (2012) 6862.
20. J. X. Hou, Z. L. Liu and P. Y. Zhang, *J. Power Sources*, 224 (2013) 139.
21. J. E. Mink, J. P. Rojas, B. E. Logan and M. M. Hussain, *Nano Lett.*, 12 (2012) 791.
22. Z. S. Lv, Y. F. Chen, H. C. Wei, F. S. Li, Y. Hu, C. H. Wei and C. H. Feng, *Electrochim. Acta*, 111 (2013) 366.
23. T. Yang, W. Zhang, M. Du and K. Jiao, *Talanta*, 75 (2008) 987.
24. E. J. Yoo, J. Kim, E. Hosono, H. S. Zhou, T. Kudo and I. Honma, *Nano Lett.*, 8 (2008) 2277.
25. U. Mehmood, *Org. Electron.*, 42 (2017) 187.
26. H. Sun, P. She, K. L. Xu, Y. X. Shang, S. Y. Yin and Z. N. Liu, *Synthetic Met.*, 209 (2015) 68.
27. R. Kakarla and B. Min, *Int. J. Hydrogen Energy*, 39 (2014) 10275.
28. A. K. Geim and K. S. Novoselov, *Nat. Mater.*, 6 (2007) 183.

29. C. Lee, X. D. Wei, J. W. Kysar and J. Hone, *Science*, 321 (2008) 385.
30. X. M. Zhang, K. Z. Li, H. J. Li, J. H. Lu, Q. G. Fu and Y. H. Chu, *Synthetic Met.*, 193 (2014) 132.
31. S. Cotchim, P. Thavarungkul, P. Kanatharana and W. Limbut, *Electrochim. Acta*, 184 (2015) 102.
32. W. S. Hummers and R. E. Offeman, *J. Am. Chem. Soc.*, 80 (1958) 1339.
33. B. Silwana, C. van der Horst, E. Iwuoha and V. Somerset, *Thin Solid Films*, 592 (2015) 124.
34. X. Zhang, Y. C. Zhang and J. W. Zhang, *Talanta*, 161 (2016) 567.
35. L. Wang, C. K. Chua, B. Khezri, R. D. Webster and M. Pumera, *Electrochem. Commun.*, 62 (2016) 17.
36. V. Pascal, D. Laetitia, L. Joel, S. Marc and P. Serge, *Appl. Surf. Sci.*, 253 (2007) 3263.
37. S. Palacin, C. Bureau, J. Charlier, G. Deniau, B. Mouanda and V. Pascal, *Chem. Phys. Chem.*, 5 (2004) 1468.
38. S. Jampasa, W. Siangproh, K. Duangmal and O. Chailapakul, *Talanta*, 160 (2016) 113.
39. M. M. Hantel, R. Nesper, A. Wokaun and R. Kotz, *Electrochim. Acta*, 134 (2014) 459.
40. J. Yan, T. Wei, B. Shao, Z. J. Fan, W. Z. Qian, M. L. Zhang and F. Wei, *Carbon*, 48 (2010) 487.
41. S. Karna, M. Mahat, T. Y. Choi, R. Shimada, Z. M. Wang and A. Neogi, *Sci. Rep.*, 6 (2016) 36898.
42. K. H. Kim, M. H. Yang, K. M. Cho, Y. S. Jun, S. B. Lee and H. T. Jung, *Sci. Rep.*, 3 (2013) 3251.
43. K. McCann and J. Laane, *J. Mol. Struct.*, 890 (2008) 346.
44. A. J. Bard and L. R. Faulkner, *Electrochemical methods: Fundamentals and applications. 2nd ed.*, John Wiley & Sons Inc, (2001) New York, USA.
45. K. Rabaey and W. Verstraete, *Trends Biotechnol.*, 23 (2005) 291.

© 2017 The Authors. Published by ESG (www.electrochemsci.org). This article is an open access article distributed under the terms and conditions of the Creative Commons Attribution license (<http://creativecommons.org/licenses/by/4.0/>).